Applied Catalysis B: Environmental 303 (2022) 120846

Contents lists available at ScienceDirect

Applied Catalysis B: Environmental

journal homepage: www.elsevier.com/locate/apcatb

Facile synthesis of 2D covalent organic frameworks for cooperative photocatalysis with TEMPO: The selective aerobic oxidation of benzyl amines

Xia Li [a,1], Shaoxiong Yang [b,1], Fulin Zhang [a], Liyan Zheng [b], Xianjun Lang [a,*]

[a] Sauvage Center for Molecular Sciences, College of Chemistry and Molecular Sciences, Wuhan University, Wuhan 430072, China
[b] Key Laboratory of Medicinal Chemistry for Natural Resource of Ministry of Education, School of Chemical Science and Technology, Yunnan University, Kunming 650091, China

ARTICLE INFO

Keywords:
Covalent organic frameworks
Facile synthesis
Cooperative photocatalysis
TEMPO
Oxidation of amines

ABSTRACT

2D (two-dimensional) covalent organic frameworks (COFs) have recently emerged as versatile photoactive functional materials. Herein, three β-ketoenamine linked 2D COFs were assembled with 2,4,6-triformylphloroglucinol (Tp) and 4,7-bis(4-aminophenyl)-2,1,3-benzothiadiazole (BTD) as the building blocks at 150, 120, and 25 ℃ respectively, leading to Tp-BTD-150, Tp-BTD-120, and Tp-BTD-25. In particular, the facile synthesis at 25 ℃ afforded Tp-BTD-25 that featured superior activity for the photocatalytic selective aerobic oxidation of benzylamine to the other two assembled at higher temperatures. Most importantly, both the stability and activity of Tp-BTD-25 photocatalyst were augmented with exogenous 5 mol% TEMPO (2,2,6,6-tetramethylpiperidine-*N*-oxyl) to ease the transfer of electrons and protons during the oxidation of benzyl amines. Preeminently, the selective aerobic oxidation of benzyl amines into imines was established by cooperative photocatalysis of Tp-BTD-25 with TEMPO irradiated by blue LEDs (light-emitting diodes). This work underscores that crystalline 2D COFs via facile synthesis can cooperatively work with a redox mediator to steer photocatalytic selective reactions.

1. Introduction

Increasingly, crystalline porous materials with well-defined structures have played an important role in photocatalysis to carry out energy and environment-related reactions [1–6]. More recently, COFs, metal-free crystalline organic porous materials, emerge with tunable structures and versatile functions [7,8]. Thus, there has been a surge of interest in applying COFs as promising photocatalysts to embark upon demanding chemical reactions [9–14]. In particular, 2D COFs possessing planar and ordered π-π stacked structures equip them with a wide light response range, excellent charge mobility, and a long range of exciton delocalization, which are widely recognized as brilliant materials platforms for photocatalytic applications [15–22]. To date, several 2D COFs have been designed to be endowed with infusive photocatalytic activities for degradation of pollutants [23], reduction of CO_2 [24,25], and evolution of H_2 [26], etc. Additionally, most of these 2D COFs are fabricated via solvothermal synthesis, which often needs to be sealed with a thick-walled glass tube at vacuum or in an inert atmosphere, and must be placed at a high temperature for a long time. Therefore, it is highly desirable to enable the facile synthesis of 2D COFs at ambient conditions due to the merits of cost-effectiveness, green condition, and easy operation [27]. To this end, the pursuit of a suitable linkage is the key based on the reversible covalent bonds necessitated by the formation of crystalline 2D COFs.

Amongst various linkages, β-ketoenamine, due to the irreversible enol-to-keto tautomerization affords remarkable chemical stability, becoming one of the most popular linkages to construct 2D COF photocatalysts [28,29]. So far, several studies have proved β-ketoenamine linked COFs possessing good light-capturing capability and high-activity in visible light photocatalysis [30–32]. For instance, a cyano conjugated β-ketoenamine linked COF showed remarkable photocatalytic activity in H_2 evolution [33]. Very interestingly, a recent investigation demonstrated that more β-ketoenamine linkages in the COFs containing both β-ketoenamine and imine linkages exhibited better photocatalytic

* Corresponding author.
E-mail address: xianjunlang@whu.edu.cn (X. Lang).
[1] These authors contributed equally to this work

https://doi.org/10.1016/j.apcatb.2021.120846
Received 13 September 2021; Received in revised form 15 October 2021; Accepted 23 October 2021
Available online 29 October 2021

performance in H_2 evolution owing to a more favorable HOMO (highest occupied molecular orbital) level and a nonquenched excited state [34]. Additionally, the incorporation of different building blocks could endow β-ketoenamine linked COFs with appropriate redox capability to meet the requirements of various photocatalytic applications. Although the photocatalytic potential of β-ketoenamine linked COFs has gradually been discovered, their utilization in selective organic transformations is still rare [35,36]. Chiefly, the advance in their durable performance remains a big challenge. Therefore, developing capable 2D COFs for photocatalytic selective organic transformations under ambient conditions is a significant task. Encouragingly, some notable results have been furnished over 2D COFs with other linkages [37–39]. Thus, it is viable to further explore the potential of β-ketoenamine linked COFs provided one can boost their stability under photocatalytic conditions. Notably, once the mesopore of a β-ketoenamine linked COF was filled with polyethylene glycol, the photocatalytic evolution of H_2 could be boosted [40]. It is envisaged to increase the stability of β-ketoenamine linked COFs and ensuing activity by introducing a redox mediator to construct cooperative photocatalysis.

Cooperative photocatalysis that introduces a redox mediator to expedite the charge transfers of semiconductors is a resourceful approach in selective organic transformations [41]. However, this state-of-the-art paradigm often appears in inorganic semiconductor-based photocatalysts but is seldom presented in organic semiconductor photocatalysis [42]. Encouragingly, our recent study indicated that sp^2 carbon linked porphyrin-based COF is a fantastic platform for cooperative photocatalysis with TEMPO and the interesting behavior could swiftly transform amines into imines [43]. Enlightened by the successful paradigm, constructing cooperative photocatalysis between β-ketoenamine linked COFs and a redox mediator like TEMPO would be an advisable pathway in steering selective organic transformations.

Combining these leverages, herein, three β-ketoenamine linked 2D COFs were assembled with Tp and BTD as the building blocks, leading to eclipsed Tp-BTD-150, staggered Tp-BTD-120, and ABC interlayer stacked Tp-BTD-25, depending on the temperatures of synthesis. In particular, a facile synthesis at 25 ℃ afforded Tp-BTD-25 that featured superior photocatalytic activity for the selective aerobic oxidation of amines to the other two assembled at high temperatures. Most importantly, both the stability and activity of Tp-BTD-25 were augmented by adding 5 mol% TEMPO to ease the transfer of electrons and protons during the photocatalytic oxidation of amines in acetonitrile (CH_3CN). Preeminently, the selective aerobic oxidation of amines was established by cooperative photocatalysis of Tp-BTD-25 with TEMPO irradiated by blue LEDs. This work underscores that crystalline 2D COFs via facile synthesis can cooperatively work with a redox mediator to steer photocatalytic selective reactions.

2. Experimental section

2.1. Synthesis of β-ketoenamine linked 2D COFs

The three β-ketoenamine linked 2D COFs were assembled according to our previous report with slight modifications [35]. The Tp-BTD-150 and Tp-BTD-120 were fabricated via solvothermal synthesis for 72 h at 150 ℃ and 120 ℃, respectively. The detailed procedures of synthesis for Tp-BTD-150 and Tp-BTD-120 are presented in the Supplementary Data.

The facile synthesis procedure of Tp-BTD-25 is described as follows. In a 5 mL round-bottom flask, 1.0 mL *n*-butyl alcohol, 1.0 mL *o*-dichlorobenzene, 0.2 mL aqueous acetic acid (6 mol/L), 0.050 mmol Tp (10.5 mg), and 0.075 mmol BTD (24.0 mg) were added. The mixture was dispersed for 3 min of ultrasonication and then stirred at 25 ℃ for 72 h under an atmosphere of air. After centrifugation, the collected solid was washed with THF (tetrahydrofuran) and acetone several times until the supernatant turned clear. The obtained solid was dried at room temperature, and then desiccated in a vacuum chamber at 100 ℃ for 12 h to produce Tp-BTD-25 as orange-red powder.

2.2. General procedure for selective oxidation of benzyl amine by cooperative photocatalysis of Tp-BTD-25 with TEMPO

Generally, 0.3 mmol benzylamine, 5 mg Tp-BTD-25, and 0.015 mmol TEMPO were put into a 10 mL Pyrex bottle containing 1.0 mL CH_3CN. The mixture was then stirred for 0.5 h to attain an adsorption-desorption equilibrium in the dark. Thereafter, the Pyrex bottle connected to air was irradiated by blue LEDs (3 W × 4, Shenzhen Ouying Lighting Science and Technology Co., Ltd.), which was stirred simultaneously at a speed of 1500 rpm at room temperature. Upon completion, the Tp-BTD-25 nanoparticles were removed by centrifugation. Then the reaction mixture was obtained. Finally, the clear reaction mixture was analyzed with a gas chromatographer equipped with a flame ionization detector (GC–FID) using an internal standard method. Moreover, gas chromatography–mass spectrometry (GC–MS) was used to further identify the products.

3. Results and discussion

3.1. Synthesis and characterization of β-ketoenamine linked 2D COFs

To assemble stable 2D COFs, Tp and BTD were selected as the building blocks to construct β-ketoenamine linked 2D COFs (Fig. 1). Introducing an electron-withdrawing unit BTD into the framework could not only adjust the redox capability and extend the light absorption range but also improve charge mobility for the formed donor–acceptor type COFs [44–47]. Tp-BTD-25 was facilely synthesized under ambient conditions by reacting Tp with BTD in a mixture of *n*-butyl alcohol, *o*-dichlorobenzene, and aqueous acetic acid at 25 ℃ for 72 h. As a control, the β-ketoenamine linked 2D COFs were also fabricated via solvothermal synthesis at 120 ℃ (Tp-BTD-120) and 150 ℃ (Tp-BTD-150) for 72 h, respectively. The three β-ketoenamine linked 2D COFs were all isolated as orange-red powders (Fig. S1) after centrifugation and washed with THF and acetone. To verify the three β-ketoenamine linked 2D COFs, various characterizations were conducted. First, the phase purity and crystallinity of Tp-BTD-150, Tp-BTD-120, and Tp-BTD-25 were analyzed via the powder X-ray diffraction (PXRD) technique. As displayed in Fig. 2a–c, all the three β-ketoenamine linked 2D COFs exhibit diffraction peaks at low angles, revealing that highly crystalline structures were formed. These features were not found in the Tp and BTD building blocks (Fig. S2). Interestingly, the PXRD patterns of Tp-BTD-150, Tp-BTD-120, and Tp-BTD-25 were distinctly different even though they were constructed with the same building blocks. Three isomers of β-ketoenamine linked 2D COFs were produced with dissimilar stackings. The crystal model simulation

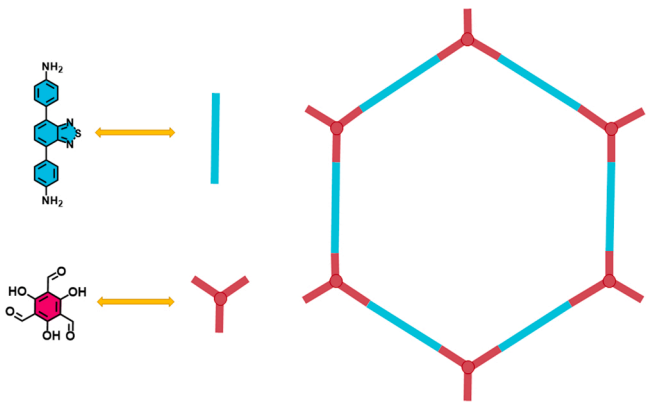

Fig. 1. Schematic representation for the β-ketoenamine linked 2D COFs.

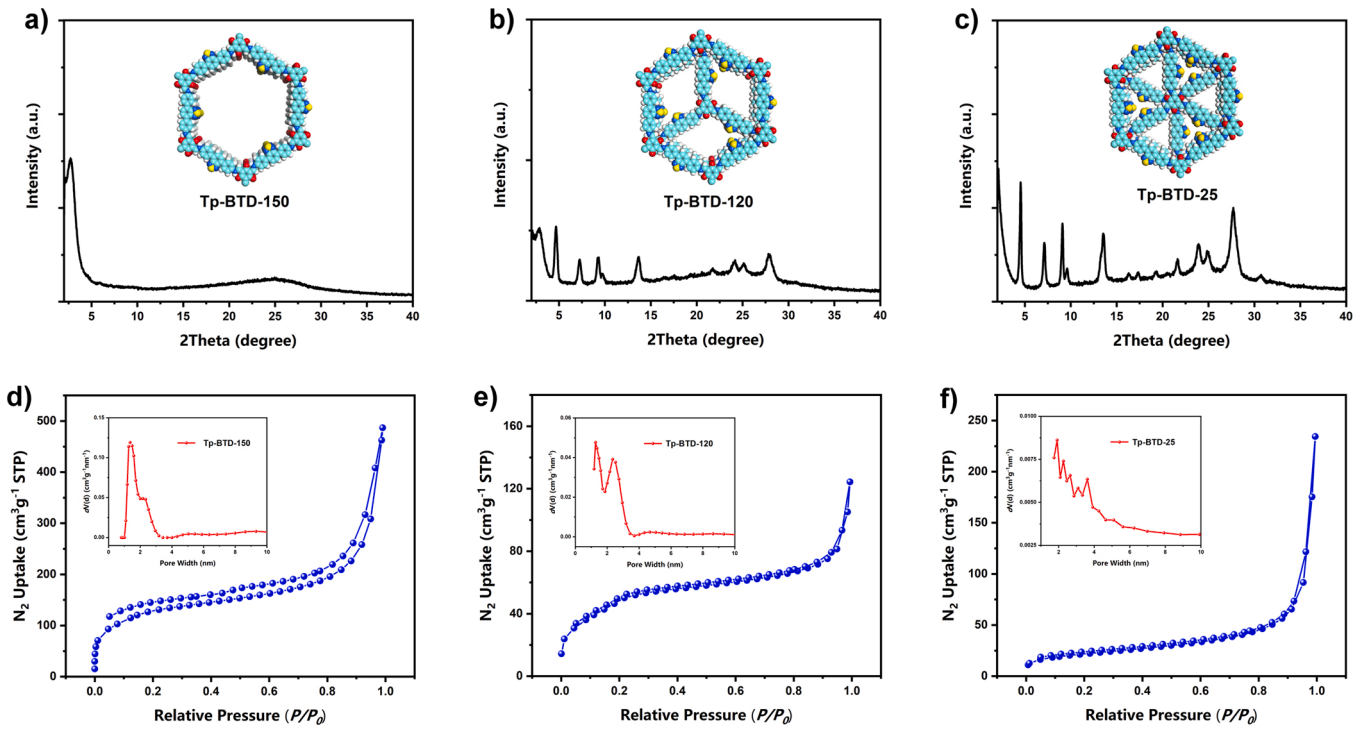

Fig. 2. PXRD patterns of a) Tp-BTD-150, b) Tp-BTD-120, c) Tp-BTD-25 and N_2 adsorption and desorption isotherms of e) Tp-BTD-150, d) Tp-BTD-120, f) Tp-BTD-25 at 77 K. Inset: pore size distributions.

[35] reveals that the experimental PXRD patterns of β-ketoenamine linked 2D COFs fabricated at 150 ℃ (Tp-BTD-150) and 120 ℃ (Tp-BTD-120) were in line with the simulated diffraction profiles afford by eclipsed stacking and staggered stacking, respectively, whilst the experimental PXRD pattern of β-ketoenamine linked 2D COF assembled at 25 ℃ (Tp-BTD-25)matched agreeably with the ABC stacking.

The permanent porosities of Tp-BTD-150, Tp-BTD-120, and Tp-BTD-25 were assessed by N_2 adsorption and desorption isotherms at 77 K. As displayed in Fig. 2d–f, the diminishing N_2 adsorption at low pressure (Tp-BTD-25 < Tp-BTD-120 < Tp-BTD-150) reveals the microporous characteristic gradually transform to a more mesoporous one as the decreases of synthesis temperature. This observation was in accord with the corresponding pore-size distribution. Accordingly, the Brunauer–Emmett–Teller (BET) specific surface areas are 460.1, 188.4, and 75.6 $m^2 g^{-1}$ for Tp-BTD-150, Tp-BTD-120, and Tp-BTD-25, respectively. The diverse stackings between the COF layers can lead to the reduced BET specific surface areas. The BET specific surface areas are important material parameters. Nevertheless, larger BET specific surface areas do not directly give rise to superior photocatalytic activity because the large molecular size of benzylamine excludes the contribution of pores smaller than 0.5 nm in aperture. Further structure and chemical composition of Tp-BTD-150, Tp-BTD-120, and Tp-BTD-25 were evidenced by the Fourier transform infrared (FTIR) spectra (Fig. S3). The signal peak at 1259, 1453, and 1621 cm^{-1} were ascribed to the characteristic vibration bands of C−N, C═C, and C═O, respectively, which proved β-ketoenamine linkages were successfully constructed. Moreover, the bathochromic shift from 1645 cm^{-1} to 1621 cm^{-1} of C═O stretching bands of Tp as well as the fading of the characteristic peak at 3500–3300 cm^{-1} attributed to N−H stretching bands of BTD also indicated the effective condensation between aldehyde groups of Tp and amino groups of BTD. The thermal stability of Tp-BTD-150, Tp-BTD-120, and Tp-BTD-25 was then tested by thermogravimetric analysis (TGA) (Fig. S4). It was found that all the COFs can be stable in the temperature of more than 300 ℃. However, the thermal stability of Tp-BTD-25 was slightly poorer than the other two fabricated at high temperatures. Scanning electron microscopy (SEM) disclosed that β-ketoenamine linked 2D COFs assembled at different temperatures possess different morphologies (Fig. S5). But all the three β-ketoenamine linked 2D COFs contains abundant porous structure. Atomic force microscopy (AFM) proved Tp-BTD-150, Tp-BTD-120, and Tp-BTD-25 were 2D materials. The average thickness measured along the line in AFM was 3.94 nm for Tp-BTD-150, 3.46 nm for Tp-BTD-120, and 5.27 nm for Tp-BTD-25, respectively (Fig. 3). Transmission electron microscopy (TEM) images clearly show all the three COFs have stacking layered structures (Fig. 4a–c). Satisfyingly, clear lattice stripes originated from the π–π stacking of COF layers can be discovered in high-resolution TEM (HRTEM) image of Tp-BTD-25 (Fig. 4d). The average lattice spacing of 0.21 nm corresponds with the distance of the COF layers, which is consistent with the theoretical calculation.

Next, the photoelectrochemical properties of Tp-BTD-150, Tp-BTD-120, and Tp-BTD-25 were investigated. From the UV–visible diffuse reflectance spectra (UV–vis DRS), the absorption profiles of the three β-ketoenamine linked 2D COFs were similar and all of them have wide absorption in the visible light region (Fig. 5a). The optical bandgaps of Tp-BTD-150, Tp-BTD-120, and Tp-BTD-25 were calculated according to the Tauc plots to be 1.97, 1.98, and 2.01 eV, respectively. Mott–Schottky measurements were then executed to estimate the lowest unoccupied molecular orbital (LUMO) levels of COFs with −0.92, −0.82, and −1.1 eV versus Ag/AgCl for Tp-BTD-150, Tp-BTD-120, and Tp-BTD-25, respectively (Fig. 5b). The higher LUMO level of Tp-BTD-25 suggests it possesses a stronger ability for electron transfer. Correspondingly, the HOMO level (vs. Ag/AgCl) was calculated. The results were approximately 1.05 eV for Tp-BTD-150, 1.16 eV for Tp-BTD-120, and 0.91 eV for Tp-BTD-25, respectively. Electrochemical impedance spectroscopy (EIS) was used to assess the electrical conductivity of the three β-ketoenamine linked 2D COFs. Tp-BTD-25 showed the smallest semicircular radius (Fig. 5c), indicating the lowest resistance in charge transfer and the best separation efficiency of photogenerated charges. The highest cathodic current in linear sweep voltammetry (LSV) curves (Fig. 5d) and the highest photocurrent response (Fig. 5e) further illustrates the Tp-BTD-25 has the best electron transfer and charge separation efficiency compared to the other two COFs. Furthermore, time-

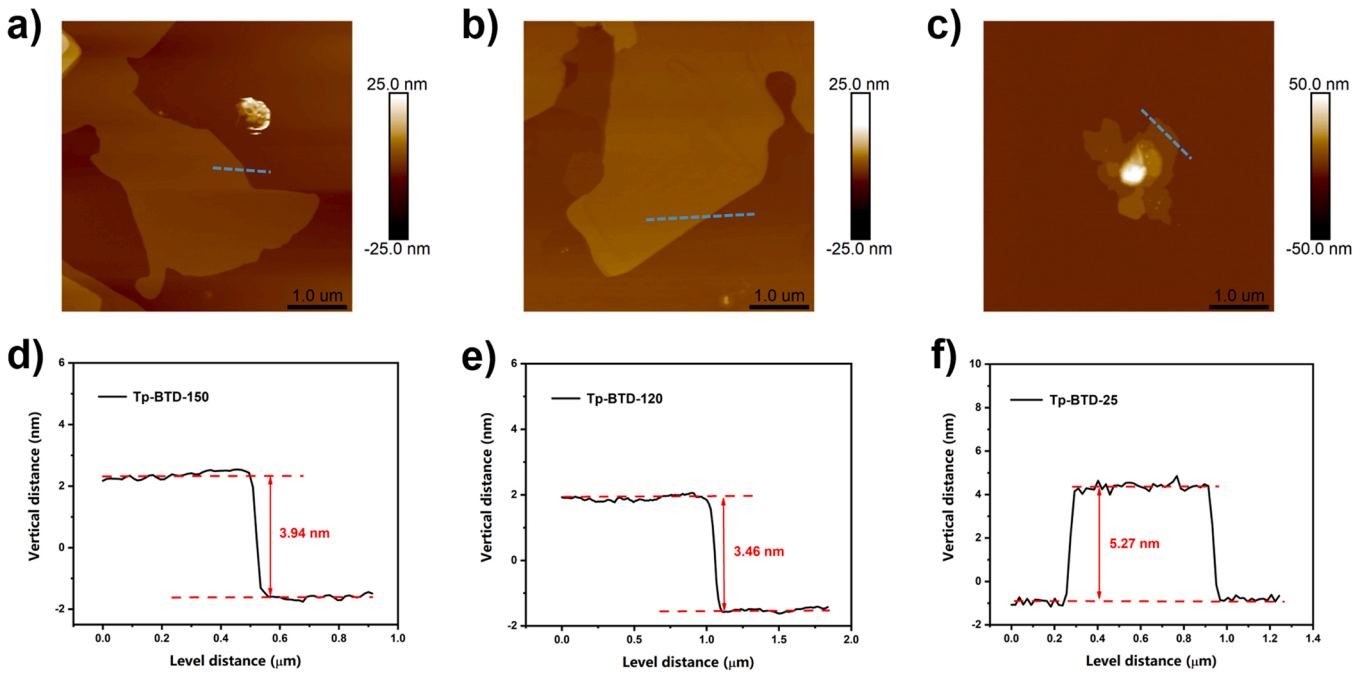

Fig. 3. AFM images of a) Tp-BTD-150, b) Tp-BTD-120, and c) Tp-BTD-25 with the measured thickness along the line shown in e) Tp-BTD-150, d) Tp-BTD-120, and f) Tp-BTD-25.

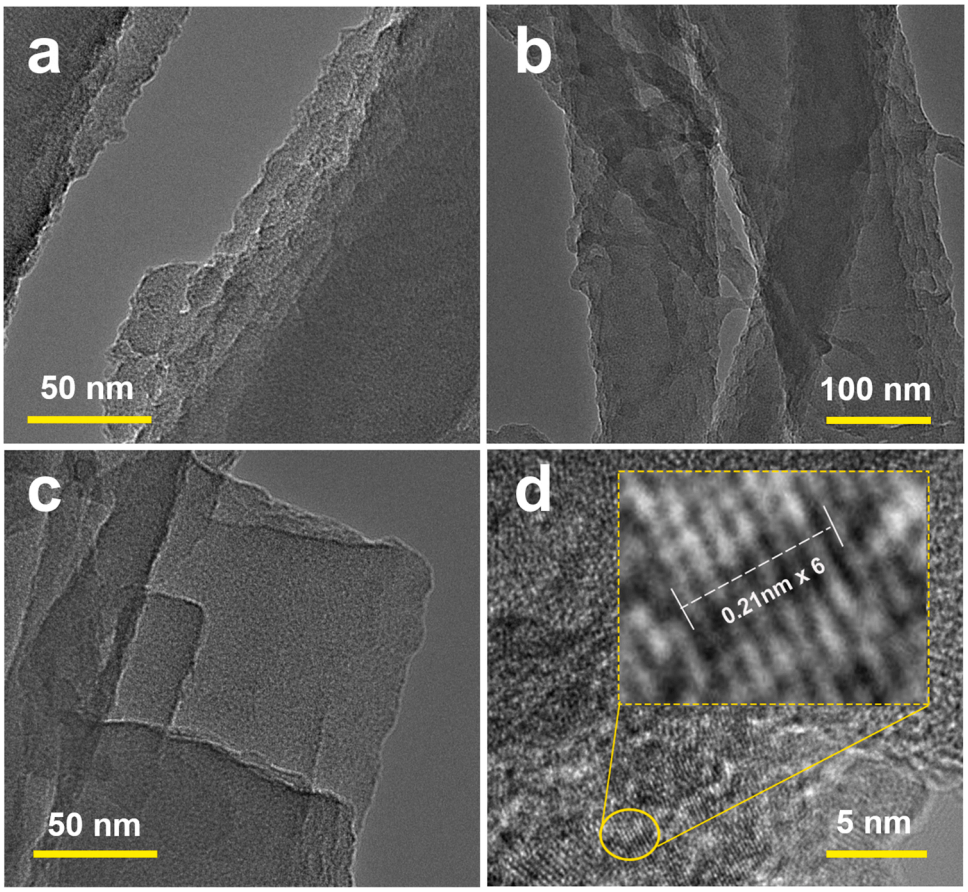

Fig. 4. TEM image of a) Tp-BTD-150, b) Tp-BTD-120, c) Tp-BTD-25 and HRTEM image of Tp-BTD-25.

resolved photoluminescence (TRPL) spectra revealed that the average TRPL lifetime of Tp-BTD-25 is the longest (Fig. 5f), which is also a vital tool to evaluate its superior charge separation efficiency. Combining the above photoelectrochemical characterization results, Tp-BTD-25 might be the best photocatalyst for selective organic transformations amongst the three COFs.

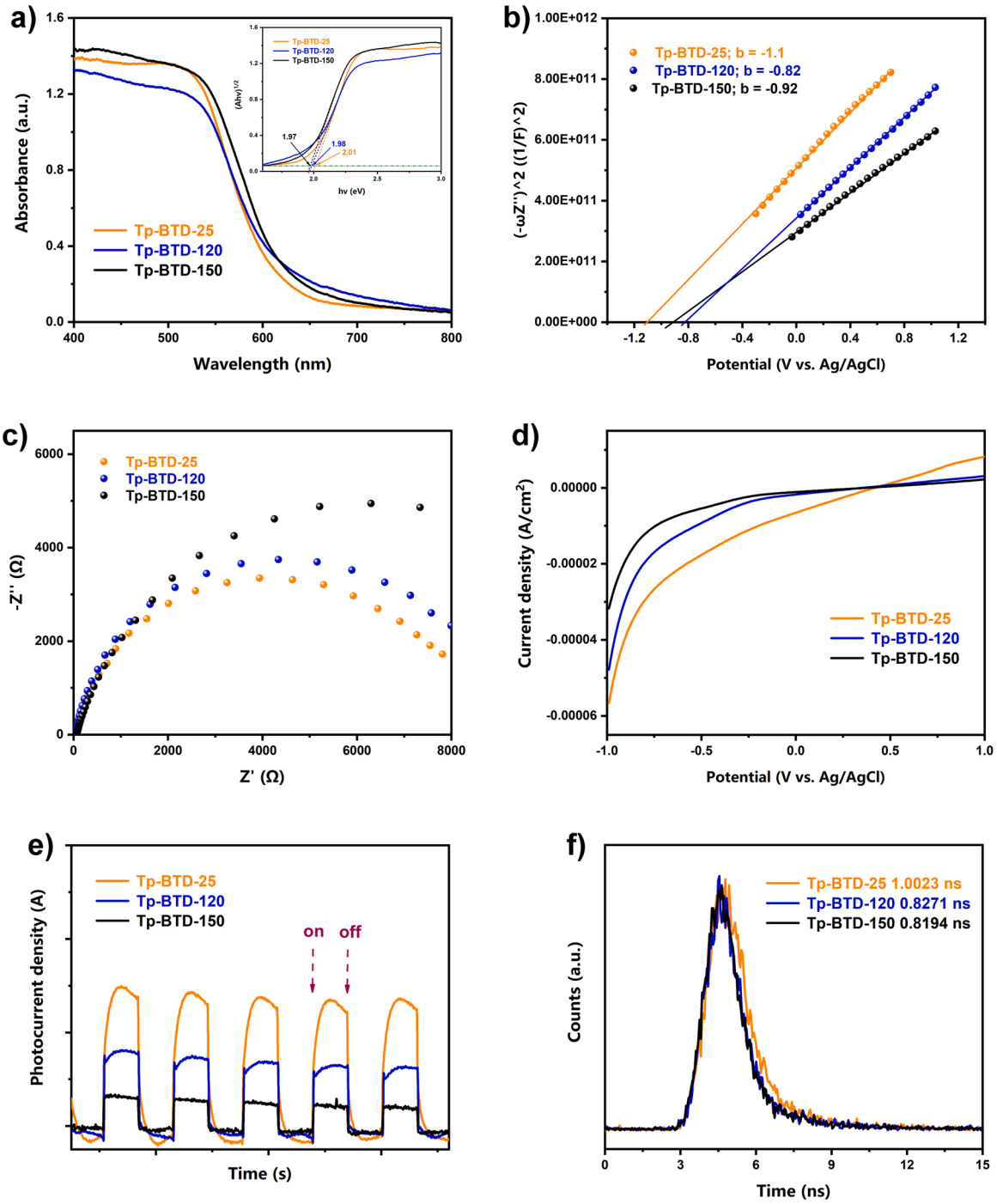

Fig. 5. a) The UV–vis DRS and the corresponding Tauc plots (inset) of Tp-BTD-150, Tp-BTD-120, and Tp-BTD-25; b) Mott-Schottky plots of Tp-BTD-150, Tp-BTD-120, and Tp-BTD-25; c) EIS of Tp-BTD-150, Tp-BTD-120, and Tp-BTD-25; d) LSV curves of Tp-BTD-150, Tp-BTD-120, and Tp-BTD-25; e) Transient photocurrents of of Tp-BTD-150, Tp-BTD-120, and Tp-BTD-25; f) TRPL spectra of Tp-BTD-150, Tp-BTD-120, and Tp-BTD-25.

3.2. Selective oxidation of benzylamine by photocatalysis of β-ketoenamine linked 2D COFs

Next, the selective aerobic oxidation of benzylamine was chosen as a probe reaction to evaluate the photocatalytic activity of the three β-ketoenamine linked COFs for which is a renewable and environmentally benign path to provide valued imines as products [48–52]. As shown in Fig. 6a, Tp-BTD-150, Tp-BTD-120, and Tp-BTD-25 displayed dissimilar photocatalytic activity in the selective oxidation of benzylamine irradiated by blue LEDs. In accord with the results of photoelectrochemical measurements, Tp-BTD-25 has the best photocatalytic performance in the oxidation of benzylamine. Nevertheless, only 42% conversion of benzylamine was obtained within 25 min reaction time. Gratifyingly, when a redox mediator, TEMPO, was presented to the system, the photocatalytic performance of Tp-BTD-25 was tremendously improved in which the conversion of benzylamine is twice as large as that without TEMPO. Similarly, the cooperative effect also appeared when employing Tp-BTD-150 or Tp-BTD-120 as photocatalysts. For the most remarkable performance of Tp-BTD-25 amongst these three β-ketoenamine linked 2D COFs, cooperative photocatalysis with TEMPO was then established based on it. Although the cooperative photocatalysis of Tp-BTD-25 with TEMPO can perform the selective oxidation

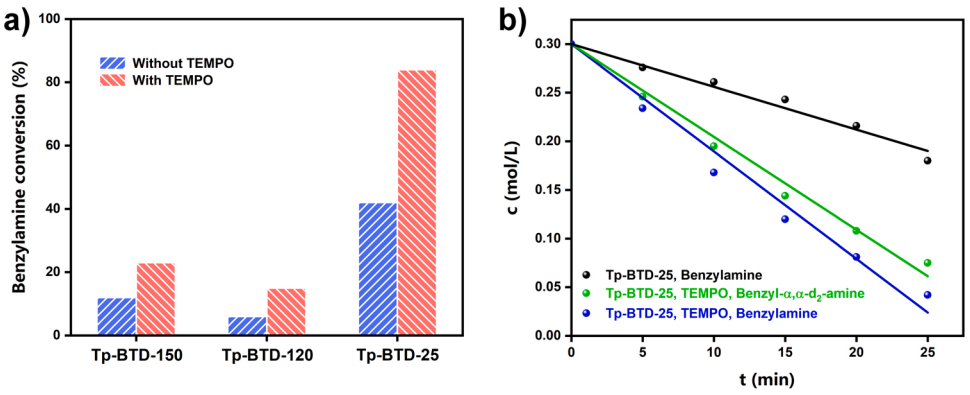

Fig. 6. a) Comparative experiments of TEMPO for the photocatalytic selective oxidation of benzylamine over β-ketoenamine linked 2D COFs, reaction conditions: benzylamine (0.3 mmol), β-ketoenamine linked 2D COF (5 mg), TEMPO (0.015 mmol), blue LEDs (3 W × 4), CH_3CN (1 mL), air (1 atm), 25 min and the underlying error estimate is ±3% calculated from three repeat experiments. b) Kinetic plots: The selective oxidation of benzylamine by Tp-BTD-25 photocatalysis (black line); The selective oxidation of benzylamine (blue line) or benzyl-α,α-d_2-amine (green line) by cooperative photocatalysis of Tp-BTD-25 with TEMPO, reaction conditions: benzylamine or benzyl-α,α-d_2-amine (0.3 mmol), Tp-BTD-25 (5 mg), TEMPO (0.015 mmol), blue LEDs (3 W × 4), CH_3CN (1 mL), air (1 atm).

of benzylamine under the whole region of visible light, the highest conversion of benzylamine was achieved with blue LEDs according to the control experiments irradiated by different LEDs (Fig. S6). Furthermore, the impact of light intensity was examined and the results uncovered the reaction is light-dependent and the conversions of benzylamine increased with the intensity of light (Table S1). Next, a series of comparative kinetic experiments were conducted. As clearly indicated in Fig. 6b, the selective oxidation of benzylamine irradiated by blue LEDs obeys zero-order kinetics. Moreover, the introduction of TEMPO significantly promoted the photocatalytic reaction rate. TEMPO can independently be a photocatalyst [53]. Here TEMPO acts a redox mediator in promoting role, resembling biological processes for oxidation of amines [54]. However, when benzylamine was replaced with benzyl-α,α-d_2-amine, the reaction rate just slightly decreased. The kinetic isotope effect (KIE) calculated by k_H/k_D with the value of 1.16 reveals that the breakage of C_α–H cannot determine the overall rate of cooperative photocatalysis.

To clarify the photocatalytic reaction mechanism, the reactive oxygen species (ROS) were next identified by adding different types of scavengers (Fig. 7a). First, when replacing O_2 with N_2, it was found that almost no imine was yielded, showing that O_2 is essential to the reaction system as the terminal oxidant. In addition, when adding *p*-benzoquinone (*p*-BQ) or $AgNO_3$, which are superoxide radical ($O_2^{\bullet-}$) or electron scavengers, the conversion of benzylamine greatly decreased, indicating the vital roles of the two species in the selective oxidation. However, no obvious decline of benzylamine conversion was observed when with CD_3CN as the solvent to extend the lifetime of singlet oxygen ($^1O_2$), suggesting $^1O_2$ does not contribute to the formation of imine. Thus, the quenching experiments disclose that $O_2^{\bullet-}$ instead of $^1O_2$ is the key ROS in this photocatalytic course. The generation of $O_2^{\bullet-}$ is a typical charge transfer process that electrons transfer from photocatalyst to O_2. The impact of O_2 pressure on the photocatalytic selective oxidation of

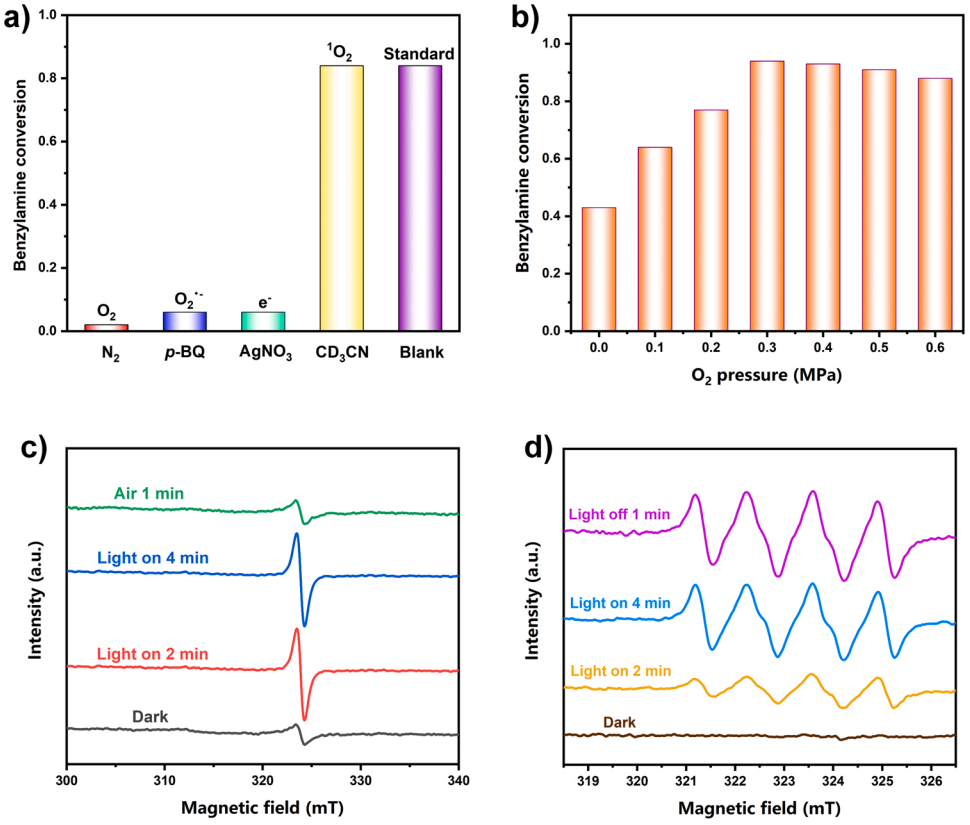

Fig. 7. a) Quenching experiments to determine the ROS , standard reaction conditions: benzylamine (0.3 mmol), Tp-BTD-25 (5 mg), TEMPO (0.015 mmol), blue LEDs (3 W × 4), CH_3CN (1 mL), air (1 atm), 25 min, or N_2 (1 atm), or *p*-BQ (0.2 equiv.), or $AgNO_3$ (1 equiv.), or CD_3CN (1 mL); b) The influence of O_2 pressure for the selective aerobic oxidation of benzylamine irradiated by blue LEDs, reaction conditions: benzylamine (0.3 mmol), Tp-BTD-25 (5 mg), TEMPO (0.015 mmol), blue LEDs (3 W × 4), CH_3CN (1 mL), 10 min; The recorded EPR spectra: c) Electrons of the Tp-BTD-25 photocatalyst; d) Spin trapping of $O_2^{\bullet-}$ with DMPO during the selective oxidation of benzylamine over Tp-BTD-25.

benzylamine (Fig. 7b) indicates that the conversion could be improved with the increased O_2 pressure but exorbitant O_2 pressure depressed the photocatalytic reaction. Subsequently, the formation of $O_2^{\bullet-}$ was further confirmed with in situ electron paramagnetic resonance (EPR) tests. The variation of LUMO electrons signal peaks of Tp-BTD-25 was presented in Fig. 7c. It was found that the LUMO electron signals gradually enlarged with continuous visible light irradiation. However, the signal intensity seriously diminished after feeding air, suggesting that electrons delivered to O_2 with the creation of $O_2^{\bullet-}$. The in situ EPR experiments with 5,5-dimethyl-pyrroline-*N*-oxide (DMPO) as a spin trapper strongly verified that $O_2^{\bullet-}$ was increasingly produced in the cooperative photocatalytic system irradiated by visible light, which was observed from the continually enhanced signal intensity (Fig. 7d).

To further disclose the mechanism of the cooperative photocatalysis, the behaviors of TEMPO in the oxidation process were also investigated. First, the impact of the quantity of TEMPO was explored on the selective aerobic oxidation of benzylamine irradiated by blue LEDs. As seen in Fig. 8a, the conversions of benzylamine were increased with the amount of TEMPO, revealing the cooperative effect created between the Tp-BTD-25 photocatalyst and TEMPO redox mediator. Besides, the effect gets better when enlarging the amount of TEMPO. Whereas, the conversion of benzylamine could not be promoted with the further improvement of the amount of TEMPO. Adding 5 mol% TEMPO achieved the best cooperative effect, suggesting that a trade-off existed between the character of the electron-proton transfer mediator and radical scavenger for TEMPO. Next, in situ EPR experiment was conducted to investigate the interchange of TEMPO in the reaction process. For TEMPO is an EPR active species, the transformation of TEMPO can be directly observed in the EPR spectrum without adding a spin trapper. As displayed in Fig. 8b, the strong signal peak of TEMPO appeared in the dark environment, but the signal intensity of TEMPO declined sharply after 4 min irradiated by visible light, which indicates that a majority of TEMPO was converted into 2,2,6,6-tetramethylpiperidine-1-oxoammonium ($TEMPO^+$) or 2,2,6,6-tetramethylpiperidin-1-ol (TEMPOH), etc. EPR inactive species. Interestingly, the signal intensity of TEMPO gradually recovered after turning off the light. The redox catalytic cycle produced by TEMPO is the key to pair with the photocatalytic cycle of Tp-BTD-25, boosting the selective oxidation of benzylamine.

Based on the above investigation, a believable mechanism for the selective aerobic oxidation of benzylamine by cooperative photocatalysis of Tp-BTD-25 with TEMPO irradiated by blue LEDs is presented in Fig. 9. First, irradiated by blue LEDs, photoexcited electrons inject into LUMO from the HOMO, producing the hole at the HOMO of Tp-BTD-25. Then, the electron reacts with O_2 to generate $O_2^{\bullet-}$, while exogenous TEMPO in CH_3CN is oxidized by the hole via collisional electron transfer to yield $TEMPO^+$, which then abstracts hydrogen-atom

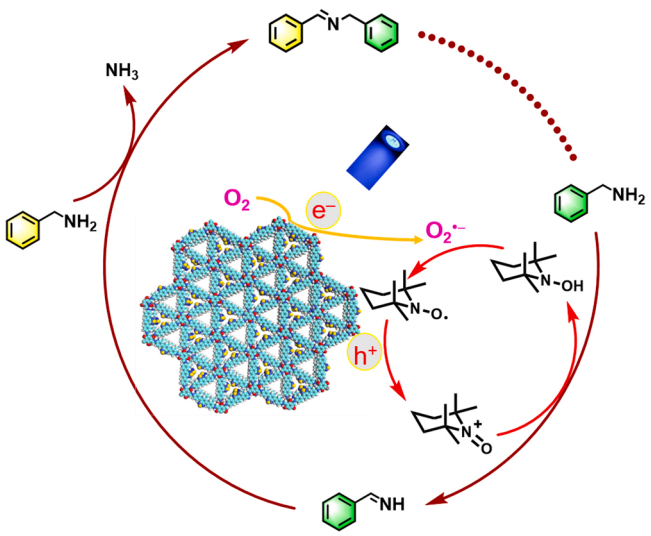

Fig. 9. The proposed mechanism for the selective aerobic oxidation of benzylamine by cooperative photocatalysis of Tp-BTD-25 with TEMPO irradiated by blue LEDs.

of benzylamine to yield benzylideneamine via a direct two-electron transfer. Finally, unreacted benzylamine couples with the yielded benzylideneamine to acquire the final product of *N*-benzylidenebenzylamine. Simultaneously, $TEMPO^+$ is converted into TEMPOH, which is then oxidized by $O_2^{\bullet-}$ to the original TEMPO to pair with the photocatalytic cycle again.

3.3. Scope of amines by cooperative photocatalysis of Tp-BTD-25 with TEMPO

Upon revealing the mechanism of cooperative photocatalysis and the explicit function of the individual components in the system, various amines were selected as substrates to check the oxidative ability of the designed system. As depicted in Table 1, all of the primary benzyl amines bearing electron-donating or electron-withdrawing groups could be effectively oxidized to desired imines with excellent selectivities (Table 1, Entries 1–9). However, the conversion of the primary amines depends on their electron effect and steric effect. The substrates with electron-donating substituents delivered significantly better outcomes than those with electron-withdrawing substituents. For instance, the benzylamines containing $–OCH_3$ or $–CH_3$ electron-donating groups (Table 1, Entries 2 and 5) were oxidized faster than these benzylamines with –F, –Cl, or –Br electron-withdrawing groups (Table 1, Entries 7–9).

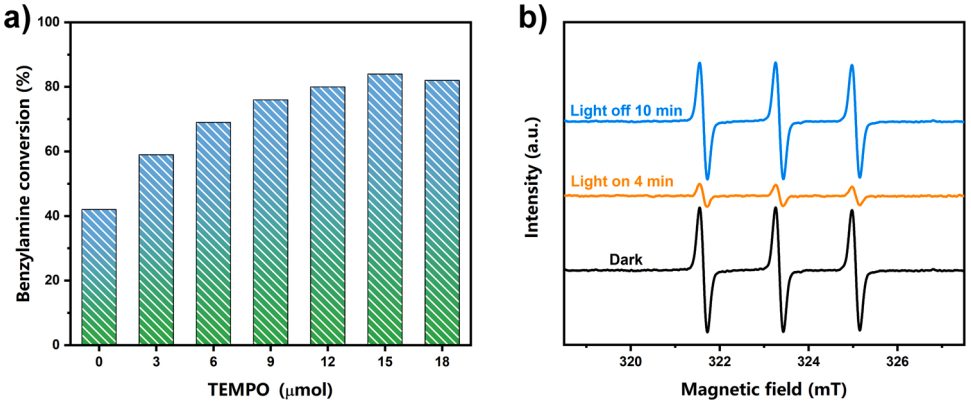

Fig. 8. a) Influence of the amount of TEMPO for the selective oxidation of benzylamine over Tp-BTD-25, reaction conditions: benzylamine (0.3 mmol), Tp-BTD-25 (5 mg), blue LEDs (3 W × 4), CH_3CN (1 mL), air (1 atm), 25 min; b) The recorded EPR spectra of TEMPO during the selective oxidation of benzylamine by cooperative photocatalysis of Tp-BTD-25 with TEMPO irradiated by blue LEDs.

Table 1
Selective aerobic oxidation of primary amines into imines by cooperative photocatalysis of Tp-BTD-25 with TEMPO irradiated by blue LEDs[a].

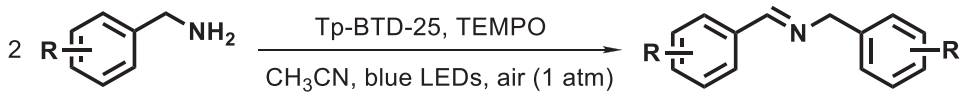

Entry	Substrate	Product	t (h)	Conv.(%) [b]	Sel.(%) [b]
1	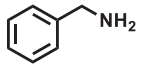	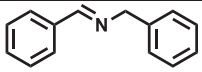	0.5	94	98
2	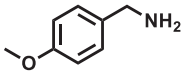	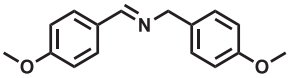	0.4	93	98
3	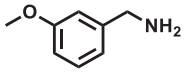	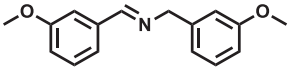	0.5	93	98
4	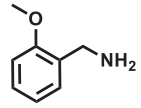	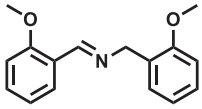	0.5	90	98
5	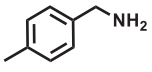	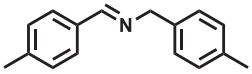	0.4	97	98
6	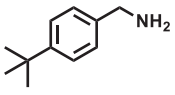	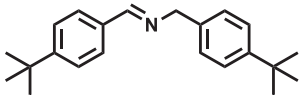	0.4	90	95
7	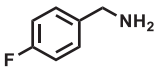	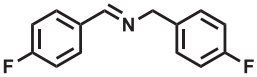	0.4	90	92
8	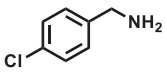	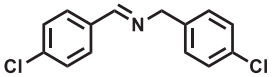	0.8	93	99
9	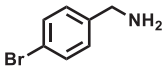	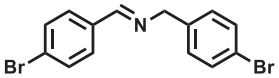	1.0	90	99
10	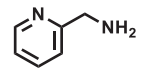	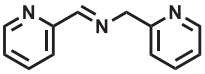	0.4	98	90
11	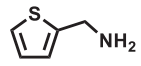	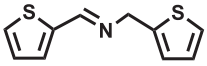	0.9	91	90

[a]Reaction conditions: primary amine (0.3 mmol), Tp-BTD-25 (5 mg), TEMPO (0.015 mmol), blue LEDs (3 W × 4), CH_3CN (1 mL), air (1 atm).
[b]Determined by GC–FID using chlorobenzene as the internal standard, conversion of primary amine, selectivity of imine.

Furthermore, when the benzylamines were incorporated with halogen groups, they have also suffered the influence of electron effect with the order of –F > –Cl > –Br. In addition, for the existence of the steric effect, 4-methoxybenzylamine displayed the higher conversion than the other two regioisomers (2-methoxybenzylamine and 3-methoxybenzylamine). The reaction followed the order of *para* > *meta* > *orth* isomer (Table 1, Entries 2–4). Notably, the *tert*-butylbenzylamine influenced by the synergy between the electronic and steric effects can also achieve good conversion (Table 1, Entry 6). Besides, heterocyclic amines encompassing N or S atoms could also be oxidized to corresponding imines (Table 1, Entries 10 and 11).

Motivated by the outstanding performance in selective oxidation of primary benzyl amines, a series of secondary benzyl amines were employed to further examine the ability of the system of cooperative photocatalysis. As shown in Table 2, all the secondary amines displayed high conversions to afford imines with good selectivities with O_2 as the oxidant. But due to the presence of bigger steric hindrances, they required more time to react. All of the secondary amines can be transformed over 90% conversion. As a prototypical secondary benzyl amine, dibenzyl amine was converted into *N*-benzylidenebenzylamine up to 99% conversion within 1 h (Table 2, Entry 1). The electronic effect and steric effect exerted a weakly influence on the selective oxidation of dibenzyl amines (Table 2, Entries 2–7) but did not work on the *N*-*tert*-butyl substituted benzylamines (Table 2, Entries 8–13). *N*-isopropyl benzylamine needed less time to be converted into the desired imine with the corresponding conversion but the selectivity is slightly lower due to the undesired activation of α-hydrogen in the isopropyl side (Table 2, Entry 14). In addition to the brilliant photocatalytic

Table 2
Selective aerobic oxidation of secondary amines into imines by cooperative photocatalysis of Tp-BTD-25 with TEMPO irradiated by blue LEDs[a].

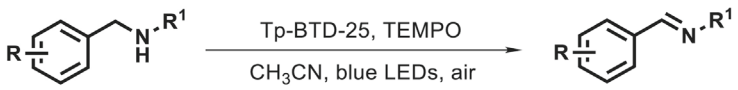

Entry	Substrate	Product	t (h)	Conv.(%) [b]	Sel.(%) [b]
1	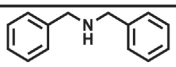	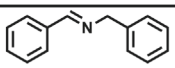	1.0	99	97
2	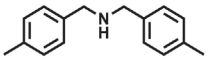	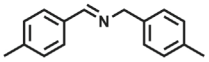	1.0	99	94
3	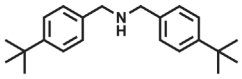	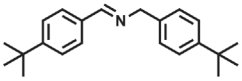	1.0	99	99
4	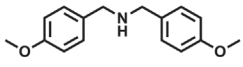	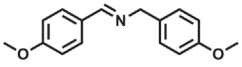	1.3	98	95
5	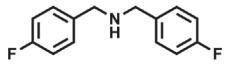	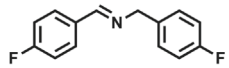	1.1	90	99
6	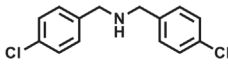	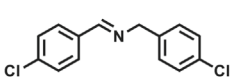	1.1	93	99
7	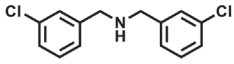	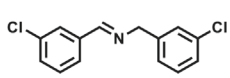	1.3	90	99
8	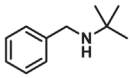	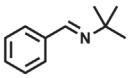	0.7	97	98
9	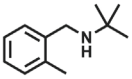	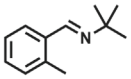	1.0	99	97
10	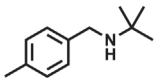	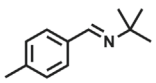	1.0	99	98
11	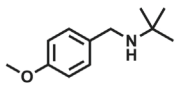	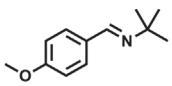	0.6	93	98
12	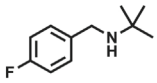	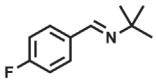	0.7	92	100
13	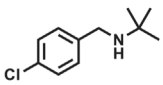	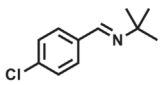	0.7	93	95
14	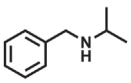	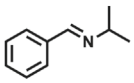	0.5	98	84

[a]Reaction conditions: secondary amine (0.15 mmol), Tp-BTD-25 (5 mg), TEMPO (0.015 mmol), blue LEDs (3 W × 4), CH_3CN (1 mL), O_2 (0.1 MPa).
[b]Determined by GC–FID using chlorobenzene as the internal standard, conversion of secondary amine, selectivity of imine.

performance, the Tp-BTD-25 photocatalyst also showed good recyclability in the selective oxidation of benzylamine (Fig. S8). After being separated from the reaction system, the reused photocatalyst still possessed a good ability to convert benzylamine.

4. Conclusions

In conclusion, three β-ketoenamine linked 2D COFs have been assembled with Tp and BTD as the building blocks at 150, 120, and 25 ℃ respectively, leading to eclipsed Tp-BTD-150, staggered Tp-BTD-120, and ABC interlayer stacked Tp-BTD-25 depending on the temperatures of synthesis. In particular, the facile synthesis at 25 ℃ afforded Tp-BTD-25 that featured significantly superior activity for the photocatalytic selective aerobic oxidation of amine to the other two assembled at high temperatures. Most importantly, both the stability and activity of Tp-BTD-25 photocatalyst were augmented by adding 5 mol% of TEMPO to ease the transfer of electrons and protons during the oxidation of amines in CH_3CN. Exceptionally, the selective aerobic oxidation of amines into imines has been established by cooperative photocatalysis of Tp-BTD-25 with TEMPO irradiated by blue LEDs. This work underscores that crystalline 2D COFs via facile synthesis can cooperatively work with a redox mediator to steer demanding photocatalytic reactions.

CRediT authorship contribution statement

Xia Li: Investigation, Writing – original draft. **Shaoxiong Yang**: Investigation, Formal analysis. **Fulin Zhang:** Investigation, Formal analysis. **Liyan Zheng:** Formal analysis, Supervision. **Xianjun Lang:** Conceptualization, Supervision, Writing – review & editing and Funding acquisition.

Declaration of Competing Interest

The authors declare that they have no known competing financial interests or personal relationships that could have appeared to influence the work reported in this paper.

Acknowledgements

This work was funded by the National Natural Science Foundation of China (grant numbers 21773173 and 22072108).

Appendix A. Supporting information

Supplementary data associated with this article can be found in the online version at doi:10.1016/j.apcatb.2021.120846.

References

[1] H. Yamashita, K. Mori, Y. Kuwahara, T. Kamegawa, M.C. Wen, P. Verma, M. Che, Single-site and nano-confined photocatalysts designed in porous materials for environmental uses and solar fuels, Chem. Soc. Rev. 47 (2018) 8072–8096, https://doi.org/10.1039/c8cs00341f.

[2] A. Dhakshinamoorthy, Z.H. Li, H. Garcia, Catalysis and photocatalysis by metal organic frameworks, Chem. Soc. Rev. 47 (2018) 8134–8172, https://doi.org/10.1039/c8cs00256h.

[3] Y. Wang, X.C. Wang, M. Antonietti, Polymeric graphitic carbon nitride as a heterogeneous organocatalyst: From photochemistry to multipurpose catalysis to sustainable chemistry, Angew. Chem. Int. Ed. 51 (2012) 68–89, https://doi.org/10.1002/anie.201101182.

[4] L. Yang, Y.T. Peng, X.D. Luo, Y. Dan, J.H. Ye, Y. Zhou, Z.G. Zou, Beyond C_3N_4 π-conjugated metal-free polymeric semiconductors for photocatalytic chemical transformations, Chem. Soc. Rev. 50 (2021) 2147–2172, https://doi.org/10.1039/d0cs00445f.

[5] Y.H. Wang, L.Z. Liu, T.Y. Ma, Y.H. Zhang, H.W. Huang, 2D graphitic carbon nitride for energy conversion and storage, Adv. Funct. Mater. 31 (2021), 2102540, https://doi.org/10.1002/adfm.202102540.

[6] Y. Chen, M.J. Xu, J.Y. Wen, Y. Wan, Q.F. Zhao, X. Cao, Y. Ding, Z.L. Wang, H.X. Li, Z.F. Bian, Selective recovery of precious metals through photocatalysis, Nat. Sustainability 4 (2021) 618–626, https://doi.org/10.1038/s41893-021-00697-4.

[7] S.Y. Ding, W. Wang, Covalent organic frameworks (COFs): From design to applications, Chem. Soc. Rev. 42 (2013) 548–568, https://doi.org/10.1039/c2cs35072f.

[8] Y.F. Zhi, Z.R. Wang, H.L. Zhang, Q.C. Zhang, Recent progress in metal-free covalent organic frameworks as heterogeneous catalysts, Small 16 (2020), 2001070, https://doi.org/10.1002/smll.202001070.

[9] H. Wang, H. Wang, Z.W. Wang, L. Tang, G.M. Zeng, P. Xu, M. Chen, T. Xiong, C. Y. Zhou, X.Y. Li, D.N. Huang, Y. Zhu, Z.X. Wang, J.W. Tang, Covalent organic framework photocatalysts: Structures and applications, Chem. Soc. Rev. 49 (2020) 4135–4165, https://doi.org/10.1039/d0cs00278j.

[10] Q. Yang, M.L. Luo, K.W. Liu, H.M. Cao, H.J. Yan, Covalent organic frameworks for photocatalytic applications, Appl. Catal. B: Environ. 276 (2020), 119174, https://doi.org/10.1016/j.apcatb.2020.119174.

[11] Y.N. Gong, W.H. Zhong, Y. Li, Y.Z. Qiu, L.R. Zheng, J. Jiang, H.L. Jiang, Regulating photocatalysis by spin-state manipulation of cobalt in covalent organic frameworks, J. Am. Chem. Soc. 142 (2020) 16723–16731, https://doi.org/10.1021/jacs.0c07206.

[12] H. Chen, W.L. Liu, A. Laemont, C. Krishnaraj, X. Feng, F. Rohman, M. Meledina, Q. Q. Zhang, R. Van Deun, K. Leus, P. van der Voort, A visible-light-harvesting covalent organic framework bearing single nickel sites as a highly efficient sulfur-carbon cross-coupling dual catalyst, Angew. Chem. Int. Ed. 60 (2021) 10820–10827, https://doi.org/10.1002/anie.202101036.

[13] X. Chen, Q. Dang, R.J. Sa, L.Y. Li, L.Y. Li, J.H. Bi, Z.Z. Zhang, J.L. Long, Y. Yu, Z. G. Zou, Integrating single Ni sites into biomimetic networks of covalent organic frameworks for selective photoreduction of CO_2, Chem. Sci. 11 (2020) 6915–6922, https://doi.org/10.1039/d0sc01747g.

[14] W.F. Zhong, R.J. Sa, L.Y. Li, Y.J. He, L.Y. Li, J.H. Bi, Z.Y. Zhuang, Y. Yu, Z.G. Zou, A covalent organic framework bearing single Ni sites as a synergistic photocatalyst for selective photoreduction of CO_2 to CO, J. Am. Chem. Soc. 141 (2019) 7615–7621, https://doi.org/10.1021/jacs.9b02997.

[15] Y.J. Zhao, H. Liu, C.Y. Wu, Z.H. Zhang, Q.Y. Pan, F. Hu, R.M. Wang, P.W. Li, X. W. Huang, Z.B. Li, Fully conjugated two-dimensional sp^2-carbon covalent organic frameworks as artificial photosystem I with high efficiency, Angew. Chem. Int. Ed. 58 (2019) 5376–5381, https://doi.org/10.1002/anie.201901194.

[16] S. Li, L. Li, Y.J. Li, L. Dai, C.X. Liu, Y.Z. Liu, J.N. Li, J.N. Lv, P.F. Li, B. Wang, Fully conjugated donor-acceptor covalent organic frameworks for photocatalytic oxidative amine coupling and thioamide cyclization, ACS Catal. 10 (2020) 8717–8726, https://doi.org/10.1021/acscatal.0c01242.

[17] F. Auras, L. Ascherl, A.H. Haldmioun, J.T. Margraf, F.C. Hanusch, S. Reuter, D. Bessinger, M. Doblinger, C. Hettstedt, K. Karaghiosoff, S. Herbert, P. Knochel, T. Clark, T. Bein, Synchronized offset stacking: A concept for growing large-domain and highly crystalline 2D covalent organic frameworks, J. Am. Chem. Soc. 138 (2016) 16703–16710, https://doi.org/10.1021/jacs.6b09787.

[18] H.V. Babu, M.G.M. Bai, M.R. Rao, Functional π-conjugated two-dimensional covalent organic frameworks, ACS Appl. Mater. Interfaces 11 (2019) 11029–11060, https://doi.org/10.1021/acsami.8b19087.

[19] S.Q. Xu, M. Richter, X.L. Feng, Vinylene-linked two-dimensional covalent organic frameworks: Synthesis and functions, Acc. Mater. Res. 2 (2021) 252–265, https://doi.org/10.1021/accountsmr.1c00017.

[20] D. Yadav, A. Kumar, J.Y. Kim, N.J. Park, J.O. Baeg, Interfacially synthesized 2D COF thin film photocatalyst: efficient photocatalyst for solar formic acid production from CO_2 and fine chemical synthesis dagger, J. Mater. Chem. A 9 (2021) 9573–9580, https://doi.org/10.1039/d1ta00802a.

[21] Y.C. Wang, H. Liu, Q.Y. Pan, C.Y. Wu, W.B. Hao, J. Xu, R.Z. Chen, J. Liu, Z.B. Li, Y. J. Zhao, Construction of fully conjugated covalent organic frameworks via facile linkage conversion for efficient photoenzymatic catalysis, J. Am. Chem. Soc. 142 (2020) 5958–5963, https://doi.org/10.1021/jacs.0c00923.

[22] H.M. Hao, F.L. Zhang, X.Y. Dong, X.J. Lang, 2D sp^2 carbon-conjugated triazine covalent organic framework photocatalysis for blue light-induced selective oxidation of sulfides with O_2, Appl. Catal. B: Environ. 299 (2022), 120691, https://doi.org/10.1016/j.apcatb.2021.120691.

[23] W.B. Chen, Z.F. Yang, Z. Xie, Y.S. Li, X. Yu, F.L. Lu, L. Chen, Benzothiadiazole functionalized D-A type covalent organic frameworks for effective photocatalytic reduction of aqueous chromium(VI), J. Mater. Chem. A 7 (2019) 998–1004, https://doi.org/10.1039/c8ta10046b.

[24] W. Huang, W. Luo, Y.G. Li, Two-dimensional semiconducting covalent organic frameworks for photocatalytic solar fuel production, Mater. Today 40 (2020) 160–172, https://doi.org/10.1016/j.mattod.2020.07.003.

[25] X.Y. Wang, Z.W. Fu, L.R. Zheng, C. Zhao, X. Wang, S.Y. Chong, F. McBride, R. Raval, M. Bilton, L.J. Liu, X.F. Wu, L.J. Chen, R.S. Sprick, A.I. Cooper, Covalent organic framework nanosheets embedding single cobalt sites for photocatalytic reduction of carbon dioxide, Chem. Mater. 32 (2020) 9107–9114, https://doi.org/10.1021/acs.chemmater.0c01642.

[26] N. Romero, R. Bofill, L. Francàs, J. García-Antón, X. Sala, Light-driven hydrogen evolution assisted by covalent organic frameworks, Catalysts 11 (2021) 754, https://doi.org/10.3390/catal11060754.

[27] A.R. Bagheri, N. Aramesh, Towards the room-temperature synthesis of covalent organic frameworks: A mini-review, J. Mater. Sci. 56 (2021) 1116–1132, https://doi.org/10.1007/s10853-020-05308-9.

[28] M. Lu, Q. Li, J. Liu, F.M. Zhang, L. Zhang, J.L. Wang, Z.H. Kang, Y.Q. Lan, Installing earth-abundant metal active centers to covalent organic frameworks for efficient heterogeneous photocatalytic CO_2 reduction, Appl. Catal. B: Environ. 254 (2019) 624–633, https://doi.org/10.1016/j.apcatb.2019.05.033.

[29] L.Y. Yin, Y.N. Zhao, Y.M. Xing, H.Q. Tan, Z.L. Lang, W.K. Ho, Y.H. Wang, Y.G. Li, Structure-property relationship in β-keto-enamine-based covalent organic

frameworks for highly efficient photocatalytic hydrogen production, Chem. Eng. J. 419 (2021), 129984, https://doi.org/10.1016/j.cej.2021.129984.
[30] B.P. Biswal, H.A. Vignolo-González, T. Banerjee, L. Grunenberg, G. Savasci, K. Gottschling, J. Nuss, C. Ochsenfeld, B.V. Lotsch, Sustained solar H_2 evolution from a thiazolo[5,4-*d*]thiazole-bridged covalent organic framework and nickel-thiolate cluster in water, J. Am. Chem. Soc. 141 (2019) 11082–11092, https://doi.org/10.1021/jacs.9b03243.
[31] S. Ghosh, A. Nakada, M.A. Springer, T. Kawaguchi, K. Suzuki, H. Kaji, I. Baburin, A. Kuc, T. Heine, H. Suzuki, R. Abe, S. Seki, Identification of prime factors to maximize the photocatalytic hydrogen evolution of covalent organic frameworks, J. Am. Chem. Soc. 142 (2020) 9752–9762, https://doi.org/10.1021/jacs.0c02633.
[32] L.L. Peng, S.Q. Chang, Z.L. Liu, Y.H. Fu, R. Ma, X.Q. Lu, F.M. Zhang, W.D. Zhu, L. C. Kong, M.H. Fan, Visible-light-driven photocatalytic CO_2 reduction over ketoenamine-based covalent organic frameworks: Role of the host functional groups, Catal. Sci. Technol. 11 (2021) 1717–1724, https://doi.org/10.1039/d0cy02061c.
[33] L.T. Wang, L.L. Zhang, B.Z. Lin, Y.Z. Zheng, J.L. Chen, Y. Zheng, B.F. Gao, J. L. Long, Y.L. Chen, Activation of carbonyl oxygen sites in β-ketoenamine-linked covalent organic frameworks via cyano conjugation for efficient photocatalytic hydrogen evolution, Small 17 (2021), 2101017, https://doi.org/10.1002/smll.202101017.
[34] H. Wang, C. Qian, J. Liu, Y.F. Zeng, D.D. Wang, W.Q. Zhou, L. Gu, H.W. Wu, G. F. Liu, Y.L. Zhao, Integrating suitable linkage of covalent organic frameworks into covalently bridged inorganic/organic hybrids toward efficient photocatalysis, J. Am. Chem. Soc. 142 (2020) 4862–4871, https://doi.org/10.1021/jacs.0c00054.
[35] S.X. Yang, X. Li, Y. Qin, Y. Cheng, W.W. Fan, X.J. Lang, L.Y. Zheng, Q.E. Cao, Modulating the stacking model of covalent organic framework isomers with different generation efficiencies of reactive oxygen species, ACS Appl. Mater. Interfaces 13 (2021) 29471–29481, https://doi.org/10.1021/acsami.1c03170.
[36] Q. Li, X.W. Lan, G.Y. An, L. Ricardez-Sandoval, Z.G. Wang, G.Y. Bai, Visible-light-responsive anthraquinone functionalized covalent organic frameworks for metal-free selective oxidation of sulfides: Effects of morphology and structure, ACS Catal. 10 (2020) 6664–6675, https://doi.org/10.1021/acscatal.0c00290.
[37] Z.P. Li, Y.F. Zhi, P.P. Shao, H. Xia, G.S. Li, X. Feng, X. Chen, Z. Shi, X.M. Liu, Covalent organic framework as an efficient, metal-free, heterogeneous photocatalyst for organic transformations under visible light, Appl. Catal. B: Environ. 245 (2019) 334–342, https://doi.org/10.1016/j.apcatb.2018.12.065.
[38] H. Liu, X.L. Yan, W.B. Chen, Z. Xie, S. Li, W.H. Chen, T. Zhang, G.L. Xing, L. Chen, Donor-acceptor 2D covalent organic frameworks for efficient heterogeneous photocatalytic α-oxyamination, Sci. China Chem. 64 (2021) 827–833, https://doi.org/10.1007/s11426-020-9931-4.
[39] R.F. Chen, J.L. Shi, Y. Ma, G.Q. Lin, X.J. Lang, C. Wang, Designed synthesis of a 2D porphyrin-based sp^2 carbon-conjugated covalent organic framework for heterogeneous photocatalysis, Angew. Chem. Int. Ed. 58 (2019) 6430–6434, https://doi.org/10.1002/anie.201902543.
[40] T. Zhou, L. Wang, X.Y. Huang, J. Unruangsri, H.L. Zhang, R. Wang, Q.L. Song, Q. Y. Yang, W.H. Li, C.C. Wang, K. Takahashi, H.X. Xu, J. Guo, PEG-stabilized coaxial stacking of two-dimensional covalent organic frameworks for enhanced photocatalytic hydrogen evolution, Nat. Commun. 12 (2021) 3934, https://doi.org/10.1038/s41467-021-24179-5.
[41] X.J. Lang, J.C. Zhao, X.D. Chen, Cooperative photoredox catalysis, Chem. Soc. Rev. 45 (2016) 3026–3038, https://doi.org/10.1039/c5cs00659g.
[42] X. Li, X.M. Ma, F.L. Zhang, X.Y. Dong, X.J. Lang, Selective photocatalytic formation of sulfoxides by aerobic oxidation of sulfides over conjugated microporous polymers with thiazolo[5,4-*d*]thiazole linkage, Appl. Catal. B: Environ. 298 (2021), 120514, https://doi.org/10.1016/j.apcatb.2021.120514.
[43] J.L. Shi, R.F. Chen, H.M. Hao, C. Wang, X.J. Lang, 2D sp^2 carbon-conjugated porphyrin covalent organic framework for cooperative photocatalysis with TEMPO, Angew. Chem. Int. Ed. 59 (2020) 9088–9093, https://doi.org/10.1002/anie.202000723.
[44] Z.A. Lan, G.G. Zhang, X. Chen, Y.F. Zhang, K.A.I. Zhang, X.C. Wang, Reducing the exciton binding energy of donor-acceptor-based conjugated polymers to promote charge-induced reactions, Angew. Chem. Int. Ed. 58 (2019) 10236–10240, https://doi.org/10.1002/anie.201904904.
[45] H.H. Ou, X.R. Chen, L.H. Lin, Y.X. Fang, X.C. Wang, Biomimetic donor-acceptor motifs in conjugated polymers for promoting exciton splitting and charge separation, Angew. Chem. Int. Ed. 57 (2018) 8729–8733, https://doi.org/10.1002/anie.201803863.
[46] C. Yang, B.C. Ma, L.Z. Zhang, S. Lin, S. Ghasimi, K. Landfester, K.A.I. Zhang, X. C. Wang, Molecular engineering of conjugated polybenzothiadiazoles for enhanced hydrogen production by photosynthesis, Angew. Chem. Int. Ed. 55 (2016) 9202–9206, https://doi.org/10.1002/anie.201603532.
[47] R. Li, J. Byun, W. Huang, C. Ayed, L. Wang, K.A.I. Zhang, Poly(benzothiadiazoles) and their derivatives as heterogeneous photocatalysts for visible-light-driven chemical transformations, ACS Catal. 8 (2018) 4735–4750, https://doi.org/10.1021/acscatal.8b00407.
[48] H.J. Chen, L.M. Peng, Y.C. Bian, X.Q. Shen, J. Li, H.C. Yao, S.Q. Zang, Z.J. Li, Exerting charge transfer to stabilize Au nanoclusters for enhanced photocatalytic performance toward selective oxidation of amines, Appl. Catal. B: Environ. 284 (2021), 119704, https://doi.org/10.1016/j.apcatb.2020.119704.
[49] J.D. Sitter, A.K. Vannucci, Photocatalytic oxidative coupling of arylamines for the synthesis of azoaromatics and the role of O_2 in the mechanism, J. Am. Chem. Soc. 143 (2021) 2938–2943, https://doi.org/10.1021/jacs.0c13101.
[50] D.R. Sun, L. Ye, Z.H. Li, Visible-light-assisted aerobic photocatalytic oxidation of amines to imines over NH_2-MIL-125(Ti), Appl. Catal. B: Environ. 164 (2015) 428–432, https://doi.org/10.1016/j.apcatb.2014.09.054.
[51] Z.L. Tian, C. Han, Y. Zhao, W.R. Dai, X. Lian, Y.N. Wang, Y. Zheng, Y. Shi, X. Pan, Z.C. Huang, H.X. Li, W. Chen, Efficient photocatalytic hydrogen peroxide generation coupled with selective benzylamine oxidation over defective ZrS_3 nanobelts, Nat. Commun. 12 (2021) 2039, https://doi.org/10.1038/s41467-021-22394-8.
[52] C. Han, Y.H. Li, J.Y. Li, M.Y. Qi, Z.R. Tang, Y.J. Xu, Cooperative syngas production and C−N bond formation in one photoredox cycle, Angew. Chem. Int. Ed. 60 (2021) 7962–7970, https://doi.org/10.1002/anie.202015756.
[53] H. Xu, Y.F. Zhang, X.J. Lang, TEMPO visible light photocatalysis: The selective aerobic oxidation of thiols to disulfides, Chin. Chem. Lett. 31 (2020) 1520–1524, https://doi.org/10.1016/j.cclet.2019.10.024.
[54] M. Largeron, M.B. Fleury, Bioinspired oxidation catalysts, Science 339 (2013) 43–44, https://doi.org/10.1126/science.1232220.